X-Ray Attenuation Coefficients for Copper in the Energy Range 5 to 50 keV

L. Gerward
Laboratory of Applied Physics III, Technical University of Denmark, Lyngby, Denmark

Z. Naturforsch. **37a**, 451–459 (1982); received February 8, 1982

Dedicated to Professor Dr. G. Hildebrandt on the occasion of his 60th birthday

X-ray mass attenuation coefficients for polycrystalline samples of copper have been measured with a high-precision energy-dispersive method. Estimates of the scattering contributions to the attenuation coefficients are made. The photoelectric coefficients deduced from the experimental results are compared with theoretical calculations using screened hydrogen-like eigenfunctions as well as more rigorous relativistic wavefunctions.

1. Introduction

The knowledge of accurate x-ray attenuation coefficients is important for the proper interpretation of experimental data in such diverse fields as x-ray powder and single crystal diffraction, x-ray fluorescence spectroscopy, electron microprobe analysis, proton induced x-ray emission, x-ray tomography, dosimetry etc. Certain discrepancies in currently available experimental data have caused the Apparatus Commission of the International Union of Crystallography to inaugurate a project aiming at improving the techniques for the measurement of attenuation coefficients and producing better sets of tables for experimenters.

Computational developments in recent years have significantly improved the theoretical description of photon interactions with atoms. Rigorous calculations of photoelectric absorption cross sections using relativistic wavefunctions have been reported by Storm and Israel [1], Cromer and Liberman [2], Scofield [3] and others. On the other hand, a theory based on Hönl's [4] and other authors' treatment of generalized scattering factors using non-relativistic hydrogen-like eigenfunctions has been shown to be in remarkably good agreement with experimental and other theoretical data in recent studies by Hildebrandt, Stephenson and Wagenfeld [5, 6, 7], Hildebrandt and Stephenson [8], Stephenson [9, 10], Gerward and Thuesen [11], Hildebrandt [12] and Gerward [13].

Reprint requests to Dr. L. Gerward, Laboratory of Applied Physics III, Building 307, Technical University of Denmark, DK-2800 Lyngby, Denmark.

The present work describes the determination of the x-ray mass attenuation coefficient of polycrystalline copper using an energy-dispersive method. Particular attention has been paid to the scattering contributions in order to deduce the proper photoelectric absorption coefficients. Two models are used for calculating the coherent scattering: A finely divided crystal powder and an assembly of independent scattering atoms. The photoelectric absorption coefficients are compared with theoretical data computed from screened hydrogen-like eigenfunctions as well as from more rigorous relativistic wavefunctions.

2. Definitions

Consider a parallel narrow beam of monochromatic x-rays passing through a plane-parallel foil of homogeneous material with surfaces normal to the beam direction and more than covering the beam cross section. The mass attenuation coefficient, μ/ϱ, is then defined by

$$\mu/\varrho = x^{-1} \ln (I_0/I) , \tag{1a}$$

where x is the mass per unit area of the foil, I_0 the incident intensity and I the emergent intensity parallel to the incident beam direction. The mass attenuation coefficient is proportional to the total photon interaction cross section per atom, σ, that is the sum of the atomic cross sections for all the elementary absorption and scattering processes. This relation is

$$\mu/\varrho = \sigma N_A/M , \tag{1b}$$

where N_A is the Avogadro number and M the atomic

0340-4811 / 82 / 0500-0451 $ 01.30/0. — Please order a reprint rather than making your own copy.

weight of the absorbing material. In the present work

$$N_A = 6.022045 \times 10^{23}\ \text{mol}^{-1} \quad \text{and}$$
$$M = 63.546\ \text{g/mol}$$

have been used.

3. Experimental Procedure

The specimens were marz grade polycrystalline copper foils (MRC, Orangeburg, New York 10962) cut into circular discs, the diameter being about 21 mm and the thickness 15 μm. The result of a spectrographic analysis is given in Table 1. A pinhole back-reflection x-ray photograph showed that the samples have a small crystallite size and exhibit a high degree of preferred orientation. The mass per unit area of each specimen was determined by weighing and by measuring the diameter along four different directions using a travelling microscope.

The experimental arrangement was described in previous works on silicon [11, 13]. Slit collimated x-rays were monochromatised by diffraction in a perfect silicon crystal. The resolution of the slit and monochromator configuration allowed the $K\alpha_1$ and $K\alpha_2$ doublet to be well resolved. The diffracted x-rays were recorded in a Si(Li) detector connected to a multichannel pulse-height analyser. Each diffraction spectrum was recorded for a certain preset lifetime, the total count rate being below 2 kcps. There was no harmonic contamination because the fundamental and the harmonic reflections from the monochromator were recorded separately in the multichannel analyser.

Table 1. Spectrographic analysis of copper specimen used in the present work.

Element	Content in ppm
H	0.6
O	1.3
N	< 0.1
Ag	< 0.3
Al	<10.0
Bi	< 0.1
Co	< 0.3
Cr	< 0.5
Fe	< 0.7
Mo	< 5.0
Ni	< 1.0
Pb	< 1.0
S	< 1.0
Si	< 0.1
Sn	< 1.0
Zn	<10.0

Absorption measurements were made for some standard $K\alpha_1$ und $K\beta_1$ lines, the $L\alpha_1$, $L\beta_1$ and $L\gamma_1$ lines of tungsten and some wavelengths of the Bremsstrahlung spectrum from the tungsten target. In the latter case the monochromator was adjusted to reflect one of the characteristic L-lines of the tungsten x-ray tube. The energies of the harmonics were thus multiples of the characteristic L-line energy chosen for the fundamental reflection. Accordingly no additional error was introduced because of any uncertainty in the energy calibration of the multichannel analyser. The intensity of the L-line, which would be prohibitively high at the power necessary for recording the harmonics, was reduced by a nickel filter. The slit collimation was chosen so that the spectral width of the Bremsstrahlung reflections was about the same as the natural width of the characteristic lines.

The number of absorbing foils was chosen to give a value of $\ln(I_0/I)$ as close as possible to 3, giving optimum attenuation conditions [14, 15]. A series of intensity measurements with the absorber in and out of the beam was taken. From these data the mean value of $\ln(I_0/I)$ and the standard deviation from the mean were calculated. The mass attenuation coefficient was then calculated from Equation (1a). Notice that the right-hand side of (1a) also contains the mass per unit area. However, it is not necessary to know the density of the sample in order to determine the mass attenuation coefficient. The relative experimental error was estimated from (1a) in the following way

$$\Delta\mu_m/\mu_m = [4(\Delta D/D)^2 + (\Delta m/m)^2 + (\Delta y/y)^2]^{1/2}, \tag{2}$$

where $\mu_m = \mu/\varrho$ and $y = \ln(I_0/I)$, ΔD and Δm are the estimated uncertainties in the determination of the foil diameter and mass, respectively, and Δy is the standard deviation from the mean mentioned above.

4. X-ray Scattering Coefficients

The scattering contribution to the narrow-beam attenuation consists of incoherent bound-electron Compton scattering (CS) and coherent scattering. *Coherence* in this context implies a fixed phase relation between the incident and scattered wave from a *single atom*.

The Compton scattering is practically insensitive to the crystalline form whereas the other components depend strongly on the crystalline state of the specimen. The coherent scattering coefficient has been calculated according to two models:

Model I: A finely divided crystal powder. The coherent scattering consists of the elastic or Laue-Bragg scattering (LBS) and the almost-elastic thermal diffuse scattering (TDS).

Model II: An assembly of independent scattering atoms. The coherent scattering consists of the Rayleigh scattering (RS).

4.1. Incoherent Scattering

The atomic cross section for the bound-electron Compton scattering, σ_{CS} is given by [16]

$$\sigma_{CS} = \pi r_e^2 \int_{-1}^{1} [1 + k(1 - \cos\varphi)]^{-2} \cdot \{1 + \cos^2\varphi + k^2(1 - \cos\varphi)^2 \cdot [1 + k(1 - \cos\varphi)]^{-1}\} I(s)\, d(\cos\varphi), \quad (3)$$

where r_e is the classical electron radius, $k = h\nu/mc^2$ i.e. the initial photon energy in electron rest-mass units, $\varphi = 2\theta$ the angle between the incident and scattered photon directions, $s = \sin\theta/\lambda$ and $I(s)$ the incoherent intensity expressed in electron units.

The incoherent intensities used in the present work were those of Cromer and Mann [17] together with the analytical approximation of Balyuzi [18]. Figure 1 shows the calculated mass attenuation coefficient due to Compton scattering as a function of energy. Also shown are the calculations of Hubbell, Veigele, Briggs, Brown, Cromer, and Howerton [19], which are seen to be in excellent agreement with the present result.

4.2. Laue-Bragg Scattering

The total power, P_H, associated with a Debye-Scherrer cone of diffracted x-rays from a sample of finely divided crystal powder can be written [20]

$$P_H = j_H I_0 Q_H \delta V, \quad (4)$$

where I_0 is the intensity of the incident beam, δV the aggregate volume of all crystallites, H stands for the reflection indices hkl and j_H is the multiplicity factor. The parameter Q_H is given by

$$Q_H = (r_e^2/V_c^2)\, C_p\, |F_H|^2 \lambda^3/4 \sin\theta, \quad (5)$$

where V_c is the volume of the unit cell, C_p the polarization factor and F_H the structure factor. In the present work unpolarized radiation will be assumed throughout, and the polarization factor becomes

$$C_p = \tfrac{1}{2}(1 + \cos^2 2\theta). \quad (6)$$

Analysis of Eq. (4) shows that Q_H represents the linear attenuation coefficient associated with the hkl reflection. The corresponding atomic cross section is obtained by dividing Q_H with the number of atoms per unit volume, or n/V_c where n is the number of atoms per unit cell. Finally, a summation over all possible hkl reflections gives the total atomic cross section, σ_{LBS}, due to Laue-Bragg scattering

$$\sigma_{LBS} = (r_e^2 \lambda^2/2 n V_c) \cdot \sum_H (C_p j d |F|^2 e^{-2M})_H, \quad (7)$$

where d_H is the spacing of the (hkl) planes. Equation (7) includes the temperature factor $\exp(-2M)$, and the Bragg equation has been used for eliminating $\sin\theta$.

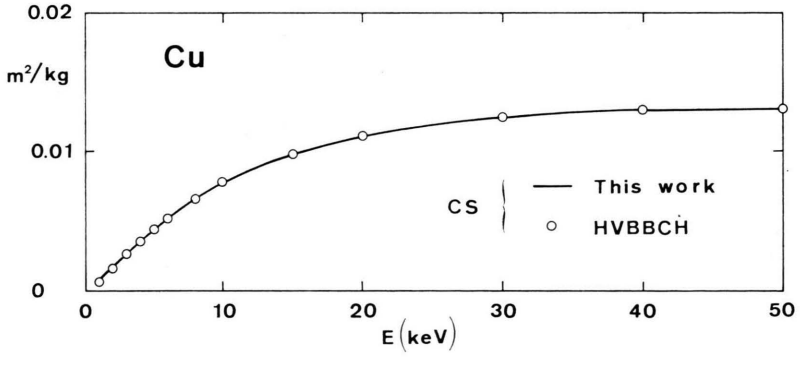

Fig. 1. Mass attenuation coefficients of copper due to Compton scattering. Full line is the calculation of the present work. Open circles denote values of Hubbell et al. [19].

4.3. Thermal Diffuse Scattering

In the approach of De Marco and Suortti [21] it is assumed that the total thermal diffuse scattering is equal to the scattering lost from the Laue-Bragg reflections because of the thermal vibrations. Comparing with (7) one obtains the following expression for the atomic cross section

$$\sigma_{\mathrm{TDS}} = (r_e^2 \lambda^2/2 n V_c) \cdot \sum_H [C_p j d |F|^2 (1 - e^{-2M})]_H . \quad (8)$$

An alternate expression can be written in the approximation of independent vibration of atoms [22]

$$\sigma_{\mathrm{TDS}} = 2\pi r_e^2 \int_{-1}^{1} C_p f^2(s)[1 - e^{-2M(s)}] \cdot d(\cos\varphi) , \quad (9)$$

where f is the atomic scattering factor.

Figure 2 shows the TDS mass attenuation coefficient of copper as a function of energy calculated according to (8) and (9), respectively. The atomic scattering factors tabulated and parametrized by Cromer and Waber [16] were extended by adding those of Hanson, Herman, Lea and Skillman for $s > 2$. The temperature factor was calculated from the Debye temperature 307 K; $V_c = 3.6148^3$ Å^3 and $n = 4$ were used.

The value of the TDS cross section according to (8) oscillates rapidly in the low-energy range as seen in Figure 2. The rapid variations occur when new Bragg reflections are included in the summation (8) as the energy increases. However, the oscillations level out with increasing energy and approach the smooth curve given by (9).

4.4. Total Coherent Scattering

It follows from (7) and (9) that the cross section of Laue-Bragg scattering plus thermal diffuse scattering can be calculated from the Laue-Bragg scattering at zero temperature, i. e. by setting $\exp(-2M) = 1$ in (7):

$$\sigma_{\mathrm{LBS+TDS}} = (r_e^2 \lambda^2/2 n V_c) \cdot \sum_H (C_p j d |F|^2)_H . \quad (10)$$

Consequently, the total coherent scattering is independent of the temperature factor. The only theoretical parameter necessary for the calculations is the atomic scattering factor.

For the approximation of independent scattering atoms, the total coherent scattering is given by the Rayleigh scattering, the cross section of which can be written [16]

$$\sigma_{\mathrm{RS}} = 2\pi r_e^2 \int_{-1}^{1} C_p f^2(s) d(\cos\varphi) . \quad (11)$$

The mass attenuation coefficients for copper calculated according to (10) and (11) are shown in Figure 3. Also shown are the calculations of Hubbell and Øverbø [24], which are seen to be in excellent agreement with the present results.

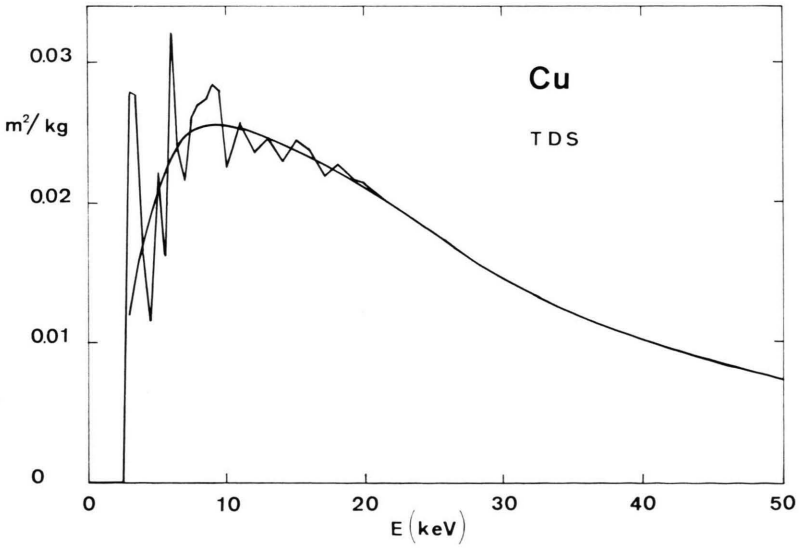

Fig. 2. Mass attenuation coefficients of copper due to thermal diffuse scattering. Oscillating curve — equation (8): smooth curve — equation (9).

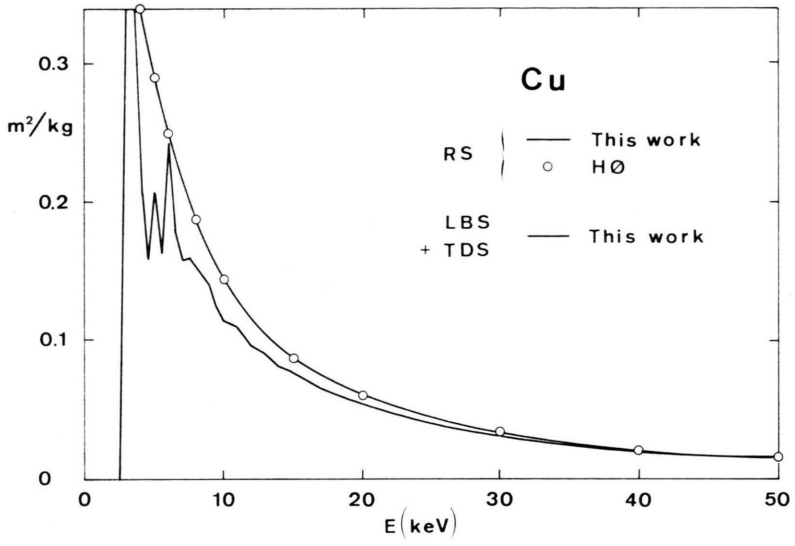

Fig. 3. Mass attenuation coefficients of copper due to coherent scattering. Oscillating curve — Laue-Bragg scattering plus thermal diffuse scattering (equ. (10)); smooth curve — Rayleigh scattering (equ. (11)). Full lines are calculations of the present work. Open circles denote values of Hubbell & Øverbø [24].

Again, the summation of the Laue-Bragg reflections causes large oscillations in the low-energy range (cf. Figure 2). The oscillations level out as the energy increases but the cross sections are consistently lower than those given by the Rayleigh scattering. A possible explanation would be that the Rayleigh scattering is forward peaked, and only few Laue-Bragg reflections are excited in the low-angle range. Therefore some intensity is suppressed by destructive interference in the crystalline absorber. Table 2, finally, shows some mass attenuation coefficients due to the total scattering (incoherent plus coherent) according to the two models discussed above: I. A finely divided crystal powder; II. Independent scattering atoms.

Table 2. Total mass scattering coefficients in units of m^2/kg for copper. Model I (LBS + TDS + CS): Laue-Bragg plus thermal diffuse plus Compton scattering. Model II (RS + CS): Rayleigh plus Compton scattering. The calculated atomic cross sections have been converted to mass attenuation coefficients using Equation (1b).

Line	E (keV)	Model I LBS + TDS + CS	Model II RS + CS
Fe $K\alpha_1$	6.404	0.184	0.241
Co $K\alpha_1$	6.930	0.161	0.224
Cu $K\alpha_1$	8.048	0.152	0.193
Mo $K\alpha_1$	17.479	0.064	0.083

5. Results and Discussions

The experimental attenuation coefficients are summarized in Table 3. It is seen that the relative experimental error is below 1% in all cases where characteristic x-ray lines have been used. The uncertainty in the determination of the specimen diameter is the main contribution in these cases. Measurements using the Bremsstrahlung are also satisfactory for energies below about 40 keV, the relative experimental error being less or only slightly larger than 1%. Above 40 keV the experimental error increases drastically. There are several factors contributing to this impairment: The high-energy limit of the x-ray generator is approached, the efficiency of the Si(Li) detector becomes low and the reflectivity of the monochromator for the highest-order harmonics is small.

Figure 4 presents the results in a graphical form together with recent experimental data from the literature [25—51]. In the medium energy range from 5 to 25 keV the mass attenuation coefficients of the present work are approximately proportional to $E^{-2.86}$ for energies below the K absorption edge and to $E^{-2.71}$ above the edge.

Table 4 shows a comparison with published data for some characteristic x-ray lines. Attenuation coefficients reported for the unresolved Kα doublet have been corrected using the power law mentioned above. The agreement between the experimenters is seen to be very good at energies higher than about

Table 3. Total and photoelectric mass attenuation coefficients in units of m^2/kg for copper. The experimental photoelectric mass attenuation coefficients of the present work are compared with theoretical values calculated according to HSW — Hildebrandt, Stephenson & Wagenfeld [6], CL/SI — Cromer & Liberman [2]/ Storm & Israel [1] and Sc — Scofield [3, 53]. The atomic photoelectric absorption cross sections obtained from the theory have been converted to mass absorption coefficients using (1b).

		This work		Theory (photo.)		
Line	E (keV)	Total	Photo	HSW	CL/SI	Sc
Fe $K\alpha_1$	6.404	9.78 (7)	9.54 (8)	9.25	9.18	9.12
Co $K\alpha_1$	6.930	7.77 (5)	7.55 (6)	7.36	7.36	7.32
Co $K\beta_1$	7.649	5.79 (4)	5.59 (5)	5.53	5.59	5.56
Cu $K\alpha_1$	8.048	5.02 (3)	4.83 (4)	4.78	4.84	4.82
W $L\alpha_1$	8.398	4.45 (3)	4.27 (4)	4.22	4.30	4.28
Cu $K\beta_1$	8.905	3.78 (3)	3.60 (4)	3.56	3.64	3.63
W $L\beta_1$	9.672	24.29 (12)	24.14 (12)	24.09	23.37	23.21
W $L\gamma_1$	11.286	15.90 (10)	15.77 (10)	16.03	15.63	15.42
white	16.795	5.51 (5)	5.42 (5)	5.49	5.36	5.32
Mo $K\alpha_1$	17.479	4.89 (3)	4.81 (3)	4.92	4.80	4.77
white	19.345	3.71 (3)	3.64 (3)	3.73	3.62	3.60
Mo $K\beta_1$	19.608	3.57 (3)	3.49 (3)	3.59	3.48	3.47
white	22.572	2.43 (2)	2.37 (3)	2.43	2.34	2.34
white	25.193	1.794 (13)	1.738 (15)	1.791	1.703	1.710
white	29.017	1.173 (16)	1.125 (17)	1.206	1.136	1.140
white	33.590	0.785 (14)	0.744 (15)	0.799	0.744	0.747
white	33.858	0.762 (9)	0.722 (10)	0.782	0.727	0.731
white	38.689	0.53 (2)	0.50 (2)	0.54	0.49	0.50
white	41.988	0.42 (4)	0.39 (4)	0.43	0.39	0.39
white	45.144	0.34 (3)	0.31 (3)	0.35	0.31	0.31

10 keV, whereas some discrepancies are observed at lower energies. Thus for Mo $K\alpha_1$ radiation (17.479 keV) the values quoted in Table 4 gives a mean value of 48.8 cm^2/g with a standard deviation of 0.4 cm^2/g or 0.75% in relative units. The difference between the largest and the smallest value is 3.0% of the mean value. The corresponding data for Cu $K\alpha_1$ radiation (8.048 keV) show a con-

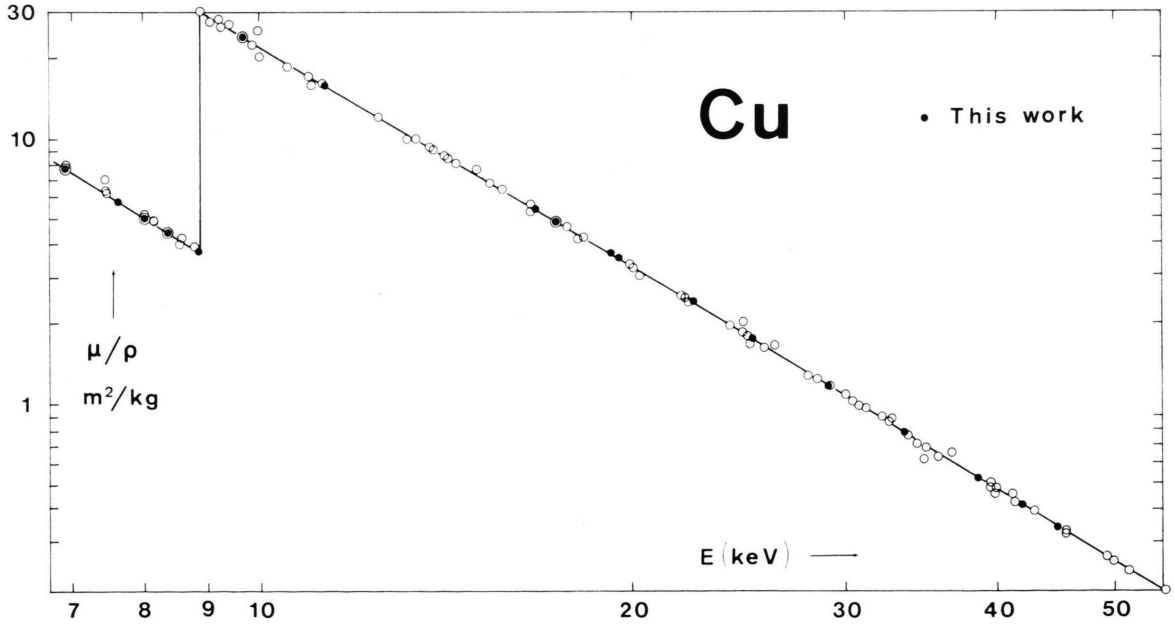

Fig. 4. Total attenuation coefficients of copper. Filled circles denote measurements of the present work, open circles experimental values from the literature [25—51].

Table 4. Comparison of experimental mass attenuation coefficients in units of cm^2/g for copper at some characteristic x-ray energies. Also included are values from the International Tables [16], denoted IT. Linear attenuation coefficients, μ, given in Refs. [35, 36] and [41] have been converted to mass attenuation coeffidcients, μ/ϱ, using $\varrho = 8.932\ g/cm^3$.

Line	Present work	Published data				
Fe $K\alpha_1$	97.8 ± 0.7	96.7 [25]	97.1 [30]	95.8 [33]	101.1 [46]	97.2 IT
Co $K\alpha_1$	77.7 ± 0.5	77.0 [33]	79.9 [39]	78.1 IT		
Cu $K\alpha_1$	50.2 ± 0.3	50.0 [25]	51.2 [26]	50.1 [32]	51.8 [33]	52.3 [34]
		50.5 [35]	49.8 [36]	52.1 [39]	49.2 [41]	51.8 [43]
		50.8 [45]	50.9 [46]	53.6 [51]	51.4 IT	
W $L\alpha_1$	44.5 ± 0.3	45.2 [26]	45.7 [45]			
Cu $K\beta_1$	37.8 ± 0.3	38.4 [26]	37.9 [29]	38.2 [30]	38.2 [45]	38.7 IT
W $L\beta_1$	242.9 ± 1.2	244.0 [26]	241 [45]			
Mo $K\alpha_1$	48.9 ± 0.3	48.8 [26]	49.0 [27]	48.8 [31]	48.6 [32]	48.6 [33]
		48.1 [35]	48.7 [36]	49.6 [43]	48.8 [45]	49.1 IT
Mo $K\beta_1$	35.7 ± 0.2	35.7 [26]	35.8 IT			

siderably larger scatter. The mean value of all data in Table 4 is 51.0 cm^2/g with a standard deviation of 1.2 cm^2/g or 2.3%. The difference between the largest and the smallest value is nearly 9%.

Values for the photoelectric mass attenuation coefficient have been obtained by subtracting the calculated scattering contributions from the experimental attenuation coefficients. The uncertainties given in Table 3 have been estimated using the experimental errors and assuming the scattering contributions to be uncertain by $\pm 20\%$.

Relativistic photoelectric mass absorption coefficients were calculated using an interpolation program for the 5 to 22 keV range provided by Cromer and Liberman [2]. Outside this range interpolated values from the tabulation of Storm and Israel [1] were used. The original calculations of both these references are based on the code of Brysk and Zerby [52]. Relativistic absorption coefficients according to Scofield [3] are also included in Table 3. They were interpolated from a recent tabulation of Hubbell [53] and corrected for the scattering contributions.

Photoelectric absorption coefficients according to the hydrogen-like theory were calculated using the formulae for the atomic sub-shell cross sections summarized by Wagenfeld [54]. Values for the subshell screening constants were taken from Hildebrandt, Stephenson and Wagenfeld [6]. Cross sections for energies between the theoretical hydrogen-like energy eigenvalue of the K shell and the actual ionization energy of the K shell were calculated using an extension to the theory described by Hildebrandt et al. [6].

An unexpected result was obtained when subtracting the scattering contributions from the experimental attenuation coefficients. The best agreement with the rigorous theories was obtained when the coherent scattering was assumed to be Rayleigh scattering (model II) instead of Laue-Bragg scattering plus thermal diffuse scattering (model I).

For a given wavelength model II predicts a larger scattering cross section than model I (see Table 2 and Figure 3). Apparently, the use of Laue-Bragg and thermal diffuse scattering underestimates the total coherent scattering in our case. It is not likely preferred orientation alone explains the extra amount of scattered intensity. Investigations by DeMarco and Suortti [21] have confirmed that preferred orientation does not appreciably affect the total amount of Laue-Bragg scattering. However, an x-ray investigation has shown that the preferred orientation in the present case is accompanied with strong microstrains and other structural imperfections, which may give rise to additional diffuse scattering. Following this conclusion the scattering contribution to the total attenuation coefficients of the present work has been derived from (3) and (11).

The results of the rigorous relativistic theories generally agree with the experiment to within 2% in the whole energy range considered in this work (Table 3 and Figure 5). Some noteworthy deviations are observed immediately above the K absorption edge and at the lowest energies.

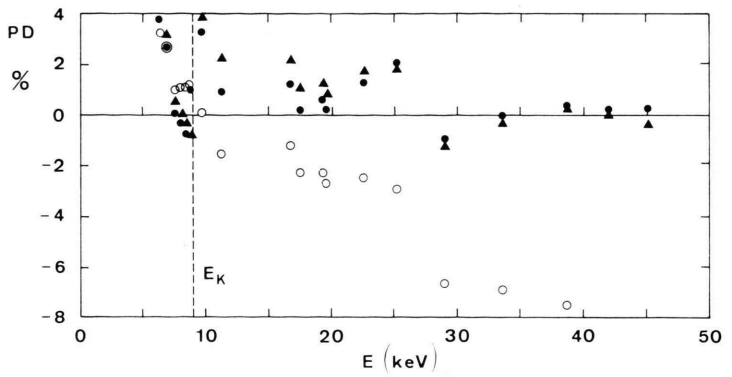

Fig. 5. Percentage difference (PD) between the photoelectric absorption coefficients of the present work and those calculated according to Hildebrandt et al. [6] (open circles), Cromer & Liberman [2]/Storm & Israel [1] (filled circles)and Scofield [3] (filled triangles).

The photoelectric absorption coefficients calculated from the hydrogen-like theory agree with the experiment to within about 2.5% in the medium energy range from 5 to 25 keV. The agreement is notably good for energies in the neighbourhood of either side of the K absorption edge. The extension to the theory described above gives a remarkably good agreement with the experiment as shown by the 9.67 keV data in Table 3 and Figure 5.

6. Conclusions

Mass absorption coefficients of polycrystalline copper have been determined with a relative experimental error of about 1% using an energy-dispersive method. It is shown that the Rayleigh scattering for independent scattering atoms also seems to be the best description of the total coherent scattering from a fine-grain polycrystalline material containing microstrain and other crystal imperfections.

Calculations of photoelectric absorption cross sections using rigorous relativistic wavefunctions are generally in good agreement with the experimental results, some deviation being observed near the high-energy side of the K absorption edge. Non-relativistic hydrogen-like calculations are in good agreement with the experimental results in the medium energy range from 5 to 25 keV, giving a remarkably good agreement close to both sides of the K absorption edge. More work is needed in the low-energy range.

Acknowledgements

Financial support from the Danish Natural Science Research Council is gratefully acknowledged. The author is indebted to Dr. D. C. Creagh for providing the specimens used in this work and to Dr. J. H. Hubbell for making his tabulation available prior to publication and for pointing out several references to the literature. Finally, the author wishes to thank Mr. B. Ribe for his all-around assistance during this project.

[1] E. Storm and H. I. Israel, Nuclear Data Tables **A 7**, 565 (1970).
[2] D. T. Cromer and D. Liberman, J. Chem. Phys. **53**, 1891 (1970); Los Alamos Scientific Laboratory Report LA-4403 (1970).
[3] J. H. Scofield, Lawrence Laboratory Report UCRL-51326 (1973).
[4] H. Hönl, Ann. Physik **18**, 625 (1933); Z. Physik **84**, 1 (1933).
[5] G. Hildebrandt, J. D. Stephenson, and H. Wagenfeld, Z. Naturforsch. **28a**, 588 (1973).
[6] G. Hildebrandt, J. D. Stephenson, and H. Wagenfeld Z. Naturforsch. **30a** 697 (1975).
[7] G. Hildebrandt, J. D. Stephenson, and H. Wagenfeld, phys. stat. sol. (a) **30**, K49 (1975).
[8] G. Hildebrandt and J. D. Stephenson, Z. Naturforsch. **30a**, 1493 (1975).
[9] J. D. Stephenson, Z. Naturforsch. **30a**, 1133 (1975).
[10] J. D. Stephenson, Z. Naturforsch. **31a**, 887 (1976).
[11] L. Gerward and G. Thuesen, Z. Naturforsch. **32a**, 588 (1977).
[12] G. Hildebrandt, Acta Cryst. A **35**, 696 (1979).
[13] L. Gerward, J. Phys. B: At. Mol. Phys. **14**, 3389 (1981).
[14] M. E. Rose and M. M. Shapiro, Phys. Rev. **74**, 1853 (1948).
[15] B. Nordfors, Ark. Fys. **18**, 37 (1960).
[16] International Tables for X-Ray Crystallography, Vol. IV, Birmingham 1974.
[17] D. T. Cromer and J. B. Mann, J. Chem. Phys. **47**, 1892 (1967).
[18] H. H. M. Balyuzi, Acta Cryst. **A 31**, 600 (1975).
[19] J. H. Hubbell, W. J. Veigele, E. A. Briggs, R. T. Brown, D. T. Cromer, and R. J. Howerton, J. Phys. Chem. Ref. Data, **4**, 471 (1975).
[20] W. H. Zachariasen, Theory of X-Ray Diffraction in Crystals, John Wiley and Sons. New York 1945.

[21] J. J. DeMarco and P. Suortti, Phys. Rev. B **4**, 1028 (1971).
[22] H. Sano, K. Ohtaka, and Y.-H. Ohtsuki, J. Phys. Soc. Japan **27**, 1254 (1969).
[23] H. P. Hanson, F. Herman, J. D. Lea, and S. Skillman, Acta Cryst. **17**, 1040 (1964).
[24] J. H. Hubbell and I. Øverbø, J. Phys. Chem. Ref. Data **8**, 69 (1979).
[25] C. L. Andrews, Phys. Rev. **54**, 994 (1938).
[26] R. D. Deslattes, Dissertation, John Hopkins University, Baltimore, Md 1959.
[27] B. W. Battermann, D. R. Chipman, and J. J. DeMarco, Phys. Rev. **122**, 68 (1961).
[28] M. Wiedenbeck, Phys. Rev. **126**, 1009 (1962).
[29] H. Sørum, Physica Norvegica **1**, 157 (1963).
[30] J. L. Dalton and J. Golkak, Canadian Spectroscopy **14**, 171 (1969).
[31] L. D. Jennings, D. R. Chipman, and J. J. DeMarco, Phys. Rev. **135**, A 1612 (1964).
[32] V. N. Karev, Zavod. Lab. **30**, 548 (1964) (in russian), translated in Industr. Lab. **30**, 686 (1964).
[33] M. J. Cooper, Acta Cryst. **18**, 813 (1965).
[34] A. J. Bearden, J. Appl. Phys. **37**, 1681 (1966).
[35] S. Hosoya and T. Yamagishi, J. Phys. Soc. Japan **21**, 2638 (1966).
[36] T. O. Baldwin, F. W. Young, and A. Merlini, Phys. Rev. **163**, 591 (1967).
[37] R. P. Knerr and H. Vonach, Z. Angew. Phys. **22**, 507 (1967).
[38] J. M. McCrary, E. H. Plassmann, J. M. Puckett, A. L. Conner, and G. W. Zimmermann, Phys. Rev. **153**, 307 (1967).
[39] G. D. Hughes, J. B. Woodhouse, and I. A. Bucklow, Brit. J. Appl. Phys. (J. Phys. D) Ser. 2, **2**, 695 (1968).
[40] W. Panzer and F. Perzl, in Protection against Low Energy or Short Range Radiations and the Biological Effects of Radiation, Service Centrale de Protection contre les Rayonn. Ionisat., Le Vesinet, France 1971, p. 127.
[41] C. Ghezzi, A. Merlini, and S. Pace, Phys. Rev. B **4**, 1833 (1971).
[42] H. S. Sakota, Indian. J. Phys. **46**, 526 (1972).
[43] R. J. Temkin, V. E. Henrich, and P. M. Raccah, Phys. Rev. B **6**, 3572 (1972).
[44] R. F. Carlton and A. H. Welch, J. Tenn. Acad. Sci. (USA) **48**, 137 (1973).
[45] A. Freund in Anomalous Scattering. Edited by S. Rameseshan and S. C. Abrahams, Munksgaard International Publishers Ltd., Copenhagen 1975, p. 69.
[46] M. Mantler, X-Ray Spectrometry **3**, 90 (1974).
[47] K. Parthsaradhi and H. H. Hansen, Phys. Rev. A **10**, 563 (1974).
[48] K. Prema Chand, D. K. S. Reddy, V. Radha Krishna Murty, J. Rama Rao, and V. Lakshminarayna, J. Phys, B: At. Mol. Phys. **9**, 177 (1976).
[49] V. Radha Krishna Murty, K. Sivasankara Rao, G. Arunaprasad, K. Parthasaradhi, J. Rama Rao, and V. Lakshminarayana, Nuovo Cim. **39 A**, 125 (1977).
[50] K. S. Puttaswamy, Ramakrishna Gowda, and B. Sanjeevaiah, Can. J. Phys. **57**, 92 (1979).
[51] A. Hemidy and B. de Thy, Analusis **8**, 138 (1980).
[52] H. Brysk and C. D. Zerby, Phys. Rev. **171**, 292 (1968).
[53] J. H. Hubbell, Int. J. Appl. Rad. Isotopes, in the press.
[54] H. Wagenfeld, Phys. Rev. **144**, 216 (1966).